PLEASE CITE THIS ARTICLE AS DOI: 10.1063/5.0220000

A Multi-mass and Multi-hit Two-Camera 3D Ion Momentum Imaging System

Emmanuel Orunesajo, Sulaiman Abubakar, Blessed Oguh, Suk Kyoung Lee, and Wen Li*

Department of Chemistry, Wayne State University, Detroit, MI, 48202

*wli@chem.wayne.edu

Abstract: We demonstrate an improved two-camera system for multi-mass and multi-hit three-dimensional (3D) momentum imaging of ions. The imaging system employs two conventional complementary metal-oxide semiconductor (CMOS) cameras. We have shown previously that the system can time slice ion Newton spheres with a time resolution of 8.8 ns, limited by camera timing jitter (*J. Chem. Phys.*, **158**, 191104 (2023)). In this work, a jitter correction method was developed to suppress the camera jitter and improve the time resolution to better than 2 ns. With this resolution, full 3D momentum distributions of ions can be obtained. We further show this method can detect two ions with different masses when utilizing both the rising and falling edges of the cameras.

Introduction

3D momentum imaging of ions involves the measurement of the momentum vectors of ion fragments arising from the dissociation/ionization of molecules upon activation by photons or other energetic particles. This is usually achieved with a time and position-sensitive detector, e. g. a delay-line detector and others¹⁻⁶. Velocity map imaging (VMI) was initially developed as a 2D momentum imaging technique^{7, 8}, which employs a microchannel plate (MCP)/Phosphor screen 2D imaging detector coupled with a camera. To obtain 3D momentum distributions, mathematical inversions are needed⁹⁻¹¹, or time gating of the detector was employed to obtain slices of the 3D Newton spheres of the ionic products¹²⁻¹⁴. Recently, the Li group developed the 3D-VMI technique by adding a high-speed digitizer to the conventional VMI setup, which provides the time of flight (TOF) of each particle arriving at the imaging detector¹⁵⁻²⁰. The coincidence measurement between the position and TOF provides the three coordinates (x, y, t) that are needed to obtain the 3D momentum vectors (p_x , p_y , p_z).

While the 3D-VMI setup provides excellent imaging performance, there is still a need for cost-effective approaches that can achieve 3D momentum imaging with a massive multi-hit capability comparable with that of 2D-VMI. Most recently, the Li group demonstrated a new ion slice imaging method with a sub-10 nanosecond timing resolution²¹. This method utilized two cameras timed at different delays and measured the luminescence decay of the phosphor screen to extract the TOF of

PLEASE CITE THIS ARTICLE AS DOI: 10.1063/5.0220000

particles. The development of this approach was inspired by Strasser et al, who used a fast-gated image intensifier to time the phosphor decay²². In the new approach, the image intensifier was no longer needed, and the gating was achieved by the camera shutter function. With this approach, the Li group was able to time slice methyl cations arising from the strong-field dissociative ionization of methyl iodide with a resolution of 8.8 ns. This resolution is sufficient for slice imaging but falls short of producing well-resolved 3D momentum distributions for ions with a TOF stretch of tens of nanoseconds. Because the timing resolution is mainly limited by the camera timing jitter, it was proposed that many ions are needed in a single shot to measure and suppress the jitter. This scheme is limiting and has not been implemented so far.

Here in this work, we develop a jitter correction method using a low-cost light-emitting diode (LED). The brightness of the LED was used to characterize the camera jitter. With this method, we show the two-camera imaging system can achieve a timing resolution better than 2 ns, which allows it to capture the full 3D momentum distributions of ions with a TOF stretch of 30 ns, a typical value in many VMI experiments. Also, we are able to detect and resolve two ionic fragments with different TOFs without additional cameras or timing devices by utilizing both the rising and falling edges of the cameras.

Experimental Methods

The experimental setup and the operating principle of the two-camera imaging system have been detailed in earlier publications^{21, 23, 24}. Briefly, the experiment was carried out in an ultra-high vacuum chamber housing a 5-electrode VMI spectrometer that velocity focuses ions to an imaging detector (Photonis APD-75mm with P47 phosphor screen). The laser system was a 1 kHz Ti: sapphire two-staged amplified laser system (KMLabs Red Dragon, 800nm, 28 fs, 1mJ/pulse). The output of the amplifier was spectrally broadened using a 1m long hollow core fiber with an inner diameter of 250 µm. Afterward, a set of double-angled chirp mirrors alongside a pair of fused silica wedges was used to correct the group delay dispersion (GDD) and compress the pulse in the time domain. The final pulse produced was fully characterized using a D-scan technique and the pulse duration was measured to be 4.3 fs^{25, 26}. The laser pulse was then sent into the vacuum chamber to ionize and dissociate molecular targets through strong field ionization. The gas samples used in this experiment are H₂ and CH₃I. The strong field ionization of these samples led to the generation of ions and electrons and the voltage applied on the electrodes accelerated and velocity focused the ions towards the MCP/phosphor screen detector. The particle hits on the detector created light flashes on the phosphor screen and the positions of hits on the screen (x, y) were captured by two CMOS cameras (Basler acA 720-520um). Both cameras were triggered by a delay

PLEASE CITE THIS ARTICLE AS DOI: 10.1063/5.0220000

generator (Stanford Research System DG535), which in turn was triggered by the laser pulses. The cameras were both set to a resolution of 260 ×260 pixels and were connected to a computer using USB3 cables.

In the setup, the first camera was triggered to capture the partial luminescence decay (for P47, decay time 70 ns) of the light flashes while the second camera was pulsed to capture the full luminescence decay. The intensity ratio between the cameras for the same ion events was then used to retrieve the arrival time TOF (t) of the ions. At the outside rim of the detector, a generic red LED was mounted and pointed toward the cameras (Fig. 1a). The LED was also triggered using the same delay generator with a width of 300 ns, and its luminescence falling edge was set ~100 ns after the camera shutter opening time. In this way, the brightness of the LED will flicker whenever the camera shutter jitters in time with respect to the laser pulse. By simply measuring the brightness of the LED in the first camera, the shutter time of each camera frame can be obtained. This shutter time keeps changing with a range of a few tens of nanoseconds, even if the trigger into the camera is stable in time. This jitter in shutter open time arises from the internal timing circuitry in the camera and is universally present in machine vision cameras. The LED can be easily tucked into the corner of the camera view, so it does not interfere with the ion signal. The technique was recently employed to measure the photon arrival time with a conventional camera and achieved a remarkable 0.3 ns timing resolution²⁷. It is perfectly suited here to correct the camera jitter for ion imaging.

Results and Discussion

The time resolution of the improved two-camera imaging system shown in Fig. 1a was first characterized by detecting the arrival time of electrons, which has a much smaller TOF stretch than that of ions to facilitate the characterization. The electrons were generated from strong field ionization of methyl iodide. For this experiment, the voltages of the electrostatic lens in the VMI spectrometer were switched to detect electrons. Fig. 1b shows the clear correlation between the intensity ratios and the measured shutter open time. The shutter time was obtained by integrating the brightness of the LED on each camera frame and converting it to time using a converting factor. The converting factor was extracted from a fitting function between the peaks of the LED brightness and the delays of the camera trigger signal from the delay generator. The correlation shown in Fig. 1b reveals unambiguously that the intensity ratio distribution (and thus the TOF distribution) was broadened by the camera timing jitter. However, since the jitter time is now known for each camera frame, it can be simply corrected by subtracting it from the TOF converted from the intensity ratio between two cameras for the same event.

PLEASE CITE THIS ARTICLE AS DOI: 10.1063/5.0220000

Fig. 1b also provides a direct relationship between the intensity ratio and the TOF, which is needed to convert the measured intensity ratios to TOFs. Previously we derived such a relationship to be T = $\tau \ln \Omega + C$, in which T is the TOF, Ω is the intensity ratio and τ is the decay constant of the phosphor²¹. Fig. 1b suggests the relationship in the system can be as simple as linear, at least for a short time range (20-30 ns). The corrected TOF distributions of the electrons are shown in Fig. 1c. The distribution has a FWHM of 5.6 ns (standard deviation 2.4 ns). Note this timing resolution is a convolution between the width of the electron TOF distributions and the inherent instrument resolution. The electron TOF distribution typically has an FWHM of 3-4 ns in our VMI setup, and this suggests the actual instrument resolution is well below 2 ns (standard deviation).

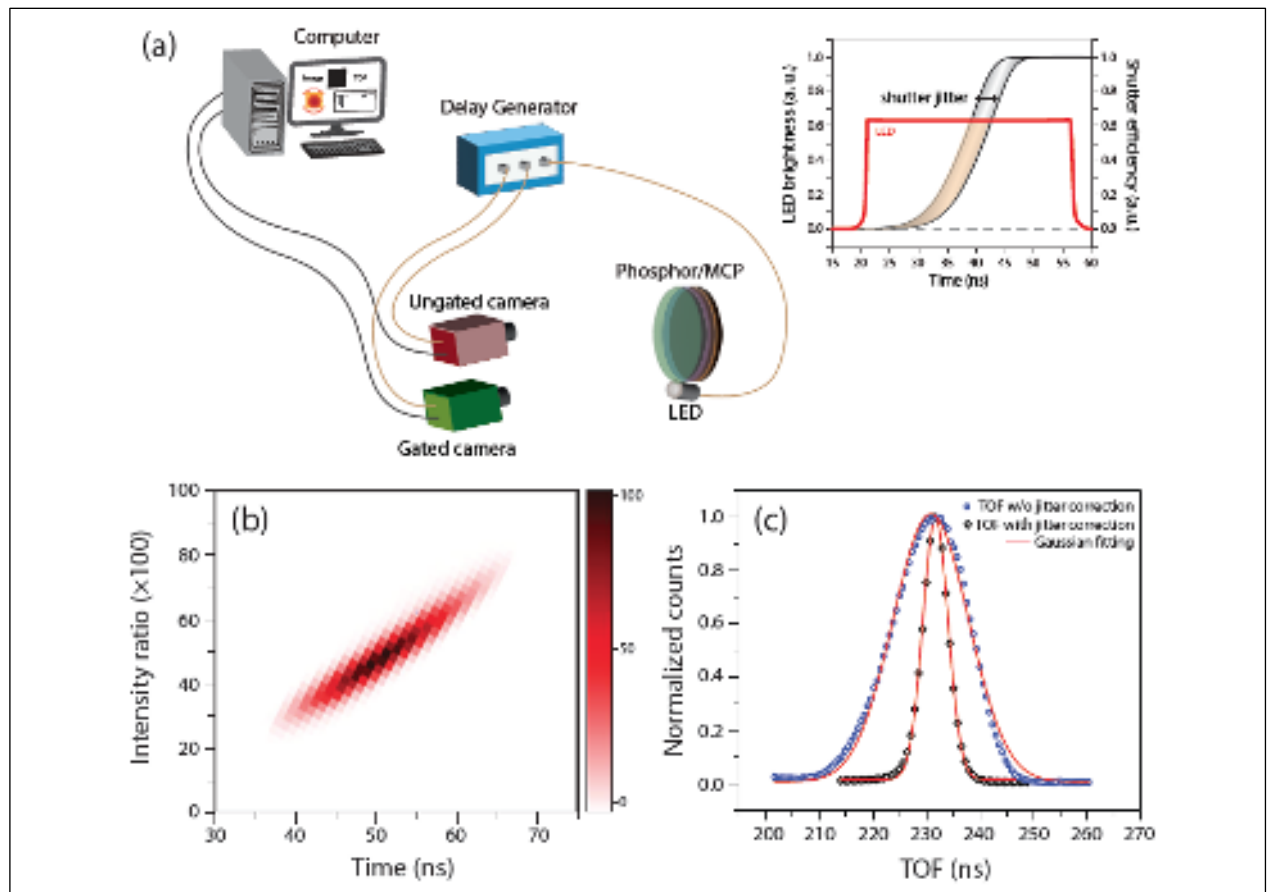


Figure 1: (a) Schematic of the two-camera imaging setup with a LED to correct camera jitter. The inset on the right shows the timing of the LED with respect to the camera shutter. Shutter efficiency is defined as the relative sensitivity of the CMOS sensor. (b) Characterization of the correlation between the intensity ratios of events and the camera shutter open time measured with LED brightness. (c) Electron TOF distributions after (black diamond) and before (blue circle) the jitter correction. Note the TOF values are relative and need to be calibrated to give the absolute TOFs. This is not done here because TOF resolution is of interest.

PLEASE CITE THIS ARTICLE AS DOI: 10.1063/5.0220000

Now we turn to detecting ions to obtain 3D momentum distributions. For this, we chose strong field dissociative single ionization of H₂ as a test system and detected H⁺ cations. The process has been the subject of many previous studies^{28, 29}. Initial ionization of H_2 gives rise to H_2^+ ground state (1s σ_g^+) and later is further excited by absorbing additional photons to the repulsive state $(2p\sigma_u^+)$, which dissociates to H⁺ and H atom. The kinetic energy release (KER) of H⁺ has a single peak located around 1 eV and its momentum distribution is highly anisotropic and lies along the laser polarization. To showcase the achieved time resolution, we first set the laser polarization horizontally along the TOF axis. In this case, the TOF distribution should show a two-peak feature due to the anisotropic momentum distribution. If we just look at the distribution of the intensity ratios obtained from the two cameras for H⁺ (Fig. 2a.), only a large broad feature is showing with a small shoulder indicating there might be additional features. This is without the jitter correction and if we were to convert this distribution directly to a TOF distribution, no two-peak feature would show up. Fig. 2b shows the correlation between the intensity ratio and the camera shutter time. The two features are seen in the 2D plot, confirming the camera jitter is the main limiting factor for the distribution in Fig. 2a. Note that the two features have different slopes, suggesting a deviation from a linear relationship between intensity ratios and shutter time. This has to be taken into consideration when converting intensity ratios to TOFs. To temporally resolve the two peaks and retrieve accurate time-of-flight information, we applied the jitter correction to each TOF value converted from the intensity ratio. The resulting TOF distribution is shown in Fig. 2c. The two peaks are now well resolved. The separation between the two peaks is about 30 ns, which makes it difficult to resolve without the jitter correction.

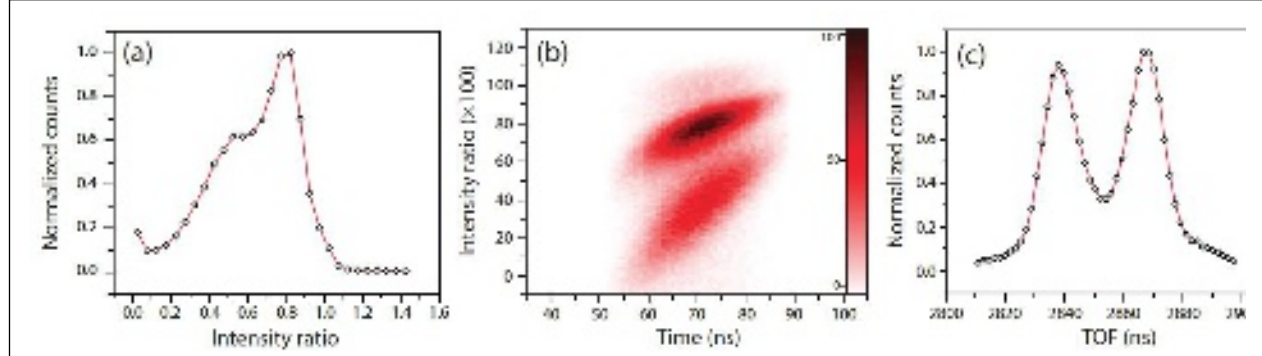


Figure 2: (a) The raw intensity ratio distribution of H⁺ ions before jitter correction (b) The correlation plot between the intensity ratio and the camera shutter time measured by the LED. (c) The jitter corrected TOF distribution of H⁺ ions.

Since we have achieved a good TOF resolution with the setup, we can now move to verify the 3D imaging performance. Figure 3a-c show the 3D momentum distributions of H⁺ cations using horizontally polarized light (along the TOF axis) while Figure 3d-f are the 3D momentum images obtained using

PLEASE CITE THIS ARTICLE AS DOI: 10.1063/5.0220000

vertically polarized light (along the Y direction). The two-lobe feature is well-resolved thanks to the good time resolution. The 3D momentum distribution shows that the laser polarization is not perfectly parallel with the TOF axis (t) of the spectrometer and has a slight tilt in both Yt and Xt directions (the X direction is horizontal but perpendicular to the TOF axis). Such information will not be available if it is not for the full 3D momentum distributions.

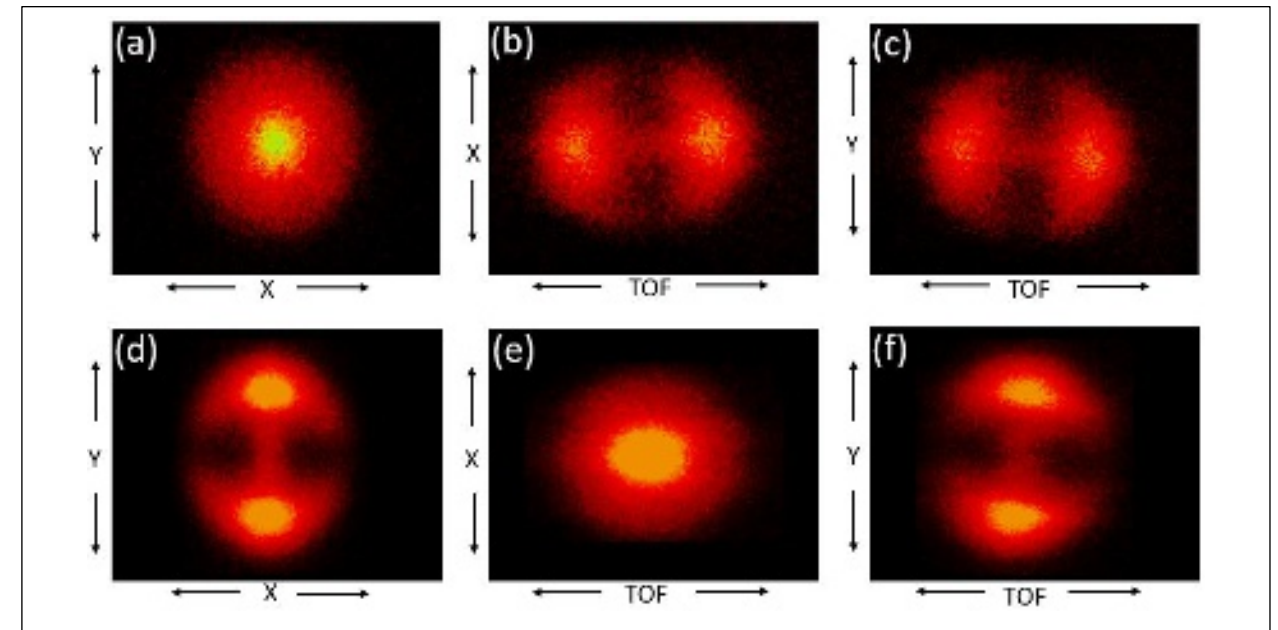


Figure 3: 3D Momentum distributions of H⁺ ions arising from the dissociative strong-field ionization of H₂ using horizontally (a, b & c) and vertically (d, e & f) polarized laser pulses. (a) and (d) are X-Y spatial views, (b) and (e) are X-t views, (c) and (f) are Y-t views.

We note that the system can detect multiple ions within a single laser shot. We have tested up to 10 counts per laser shot and the system performed well. Due to the underlying principle, as long as ion spots are well separated on cameras, the system has no fundamental limit on the number of ions it can detect. This sets the current system apart from many other 3D momentum imaging systems, which have a limited multi-hit capability including the 3D-VMI technique with considerable improvement^{30, 31}. Considering the low cost, this is a very versatile and powerful imaging system. However, the current system is not perfect and has some clear limitations too: (1) the time resolution is not high enough to resolve electron TOF yet. Further work is needed. (2) due to the short decay time of the phosphor, the TOF detection range is limited to about 100 ns for P47. It is possible to use longer decay phosphors such as P46 or P43 to extend the range. However, the achieved time resolution (Δt) might be impacted because of the relationship: $\Delta t = \frac{\tau}{DR}$, in which τ is the decay time of the phosphor and DR is the dynamic range. Due to the shot noise, the DR of the system is limited. For the cameras used here, the DR is about 140. This is estimated from the pixel full well capacity (FWC) of the camera at 20,000 electrons ($DR = \sqrt{FWC}$).

PLEASE CITE THIS ARTICLE AS DOI: 10.1063/5.0220000

This is the best-case scenario in which we assume that there are plenty of photons from the phosphor for each event. In practice, the photon number per pixel is much lower than FWC, and the DR will be much lower too. Therefore, a long decay time can result in a loss of time resolution. The detection range poses a limit on the number of different fragments the system can detect. With the P47 phosphor, the technique can practically detect a single mass. To address this issue, we previously proposed to add additional cameras that are triggered at different time delays for different masses. Here we show even with the existing two cameras, it is already possible to detect two different ions with different TOFs. This is done by setting both cameras in gating mode but at different delay times. For one mass detection, the first camera is triggered to open only after the slowest ion arrival time while the second camera is ungated, meaning the shutter opens early and closes late so it can capture the full luminescence decay of the phosphor. In this case, we are using the first camera's rising edge to gate the luminescence decay to retrieve the TOF. However, the second camera has a falling edge that can be also used to gate the luminescence. If we set the close time (falling edge) of the second camera right after the slowest arrival time of the second ion while setting the first camera's close time (falling edge) much later to capture the full luminescence decay produced by the second mass, both masses can be detected. Furthermore, because the gating/ungating are opposite for the two masses in the two cameras (Fig. 4a), the first mass will have an intensity ratio smaller than one and the second mass's intensity ratio larger than one, which makes it easy to differentiate the two masses. We can then apply corresponding conversion equations to convert the intensity ratios to TOFs. We note rising and falling edge gating requires different conversion equations to retrieve TOF. To demonstrate this arrangement, we chose to detect methyl cations (CH₃⁺) and iodine cations (I⁺) produced from dissociative single and double ionization of methyl iodide driven by intense laser fields. We also added a second LED to measure the shutter close time of the second camera. A raw intensity ratio distribution is shown in Fig. 4b. Methyl and iodine cations are well separated. The strong feature in the middle (intensity ratio ~1) is from all the ions whose TOFs are not gated by either camera. This includes residue gas ions such as water. Figure 4c shows the X-Y spatial image of the methyl and iodine cations. The inner rings are due to iodine cations from both single and double dissociative ionization and methyl cations from single dissociative ionization while the outer ring is from the methyl cation from dissociative double ionization. The black area seen in Fig. 4c is due to a mask placed on the detector to block the intense background signal from residue gas such as water. Figure 4d shows the X-t distributions of both ions. Firstly, we note the two masses are well resolved along the TOF direction and no mixing between the masses can be seen, validating our approach. Secondly, the resolution achieved with CH₃⁺ seems better than that of I⁺. This is likely because the fall time of the camera shutter is not as

PLEASE CITE THIS ARTICLE AS DOI: 10.1063/5.0220000

short as the rise time. We recently measured the rise time to be 12 ns while the fall time is close to 20 ns²⁷. A faster fall time in the camera will help with the resolution. Nonetheless, the result shows that the 3D momentum distributions of two masses can be obtained with the two-camera setup from a single measurement. Adding additional cameras is viable and the scaling is more favorable with the new scheme: with careful arrangement of delays and exposure time, a three-camera setup can measure up to four different ions, which is sufficient for many experiments. It is worth noting CMOS cameras with multi-exposure windows have started to emerge recently. Once the technology is matured, these cameras provide an easier pathway to achieve multi-mass, multi-hit 3D ion momentum imaging with the current setup. We also note the current approach provides an alternative detection scheme to the pixelated detectors such as PImMS^{32, 33} and Tpx3Cam^{18, 34} with a better or comparable timing resolution while at a fraction of the cost. However, the pixelated detectors still have the advantage of a longer TOF detecting range.

In summary, we improved the two-camera imaging system for achieving multi-mass, multi-hit 3D momentum imaging for ions. By implementing a simple jitter correction method, we were able to suppress the timing jitter between the trigger and the camera shutter opening and improve the time resolution to better than 2 ns. While the original 3D-VMI setup is designed for coincidence imaging, the two-camera setup achieves a much higher count rate thus making it a viable approach for performing covariance measurement/imaging experiments³⁵⁻³⁷.

Acknowledgment

Research supported by the National Science Foundation (NSF), CMI program, under Award # No. CHE-2107860 (method development) and the U.S. Department of Energy (DOE), Office of Science, Basic Energy Sciences (BES), under Award # DE-SC0020994 (strong field dynamics).

Reference

- ¹J. Ullrich, R. Moshammer, A. Dorn, R. Dorner, L. P. H. Schmidt and H. Schniidt-Bocking, "Recoil-ion and Electron Momentum Spectroscopy: Reaction Microscopes", Rep. Prog. Phys. **66**, 1463 (2003).
- ²R. E. Continetti, "Coincidence Spectroscopy", Ann. Rev. Phys. Chem. **52**, 165 (2001).
- ³J. Becker, K. Beckord, U. Werner and H. O. Lutz, "A system for correlated fragment detection in dissociation experiments", Nucl. Instr. Meth. Phys. Res. A **337**, 409 (1994).
- ⁴O. Jagutzki, J. S. Lapington, L. B. C. Worth, U. Spillman, V. Mergel and H. Schmidt-Böcking, "Position sensitive anodes for MCP read-out using induced charge measurement", Nucl. Instr. Meth. Phys. Res. A **477**, 256 (2002).
- ⁵C. Martin, P. Jelinsky, M. Lampton, R. F. Malina and H. O. Anger, "Wedge-and-strip anodes for centroid-finding position-sensitive photon and particle detectors", Review of Scientific Instruments **52**, 1067 (1981).

PLEASE CITE THIS ARTICLE AS DOI: 10.1063/5.0220000

- ⁶S. Loechner, Ph. D. thesis, Max-Planck-Institue for Nuclear Physics, Heidelberg, 2006.

 ⁷A. Eppink and D. Parker, "Velocity Map Imaging of Ions and Electrons Using Electrostatic Lenses:

 Application in Photoglastron and Photogramment Ion Imaging of Malassular Overgap", Pay Sci. Instrum. 68
- Application in Photoelectron and Photofragment Ion Imaging of Molecular Oxygen", Rev. Sci. Instrum. **68,** 3477 (1997).
- ⁸D. W. Chandler and P. L. Houston, "Two-dimensional imaging of state-selected photodissociation products detected by multiphoton ionization", J. Chem. Phys. **87**, 1445 (1987).
- ⁹A. J. R. Heck and D. W. Chandler, "Imaging Techniques for the Study of Chemical Reaction Dynamics", Ann. Rev. Phys. Chem. **46**, 335 (1995).
- ¹⁰M. J. Bass, M. Brouard, A. P. Clark and C. Vallance, "Fourier moment analysis of velocity-map ion images", J. Chem. Phys. **117**, 8723 (2002).
- ¹¹T. Peter Rakitzis, "Direct measurement of photofragment alignment from unnormalized Abel-invertible images", Chem. Phys. Lett. **342**, 121 (2001).
- ¹²D. Townsend, M. P. Minitti and A. G. Suits, "Direct current slice imaging", Rev. Sci. Instrum. **74,** 2530 (2003).
- ¹³J. J. Lin, J. Zhou, W. Shiu and K. Liu, "Application of time-sliced ion velocity imaging to crossed molecular beam experiments", Rev. Sci. Instrum. **74**, 2495 (2003).
- ¹⁴C. R. Gebhardt, T. P. Rakitzis, P. C. Samartzis, V. Ladopoulos and T. N. Kitsopoulos, "Slice imaging: A new approach to ion imaging and velocity mapping", Rev. Sci. Instrum. **72**, 3848 (2001).
- ¹⁵G. A. Stewart, P. Hoerner, D. A. Debrah, S. K. Lee, H. B. Schlegel and W. Li, "Attosecond Imaging of Electronic Wave Packets", Phys. Rev. Lett. **130**, 083202 (2023).
- ¹⁶E. Orunesajo, G. Basnayake, Y. Ranathunga, G. Stewart, D. Heathcote, C. Vallance, S. K. Lee and W. Li, "All-Optical Three-Dimensional Electron Momentum Imaging", J. Phys. Chem. A **125**, 5220 (2021).
- ¹⁷G. Basnayake, Y. Ranathunga, S. K. Lee and W. Li, "Three-dimensional (3D) velocity map imaging: from technique to application", J. Phys. B-At. Mol. Opt. Phys. **55**, 023001 (2022).
- ¹⁸D. A. Debrah, G. A. Stewart, G. Basnayake, A. Nomerotski, P. Svihra, S. K. Lee and W. Li, "Developing a camera-based 3D momentum imaging system capable of 1 Mhits/s", Rev. Sci. Instrum. **91**, 023316 (2020). ¹⁹S. K. Lee, F. Cudry, Y. F. Lin, S. Lingenfelter, A. H. Winney, L. Fan and W. Li, "Coincidence ion imaging with a fast frame camera", Rev. Sci. Instrum. **85**, 123303 (2014).
- ²⁰Y. F. Lin, S. K. Lee, P. Adhikari, T. Herath, S. Lingenfelter, A. H. Winney and W. Li, "Note: An improved 3D imaging system for electron-electron coincidence measurements", Rev. Sci. Instrum. **86**, 096110 (2015). ²¹Y. Ranathunga, T. Olowolafe, E. Orunesajo, H. Musah, S. K. Lee and W. Li, "Slicing Newton spheres with a two-camera 3D imaging system", J. Chem. Phys. **158**, (2023).
- ²²D. Strasser, X. Urbain, H. B. Pedersen, N. Altstein, O. Heber, R. Wester, K. G. Bhushan and D. Zajfman, "An innovative approach to multiparticle three-dimensional imaging", Rev. Sci. Instrum. **71**, 3092 (2000). ²³Q. Liao, A. H. Winney, S. K. Lee, Y. F. Lin, P. Adhikari and W. Li, "Coulomb-repulsion-assisted double ionization from doubly excited states of argon", Phys. Rev. A **96**, 023401 (2017).
- ²⁴A. H. Winney, G. Basnayake, D. A. Debrah, Y. F. Lin, S. K. Lee, P. Hoerner, Q. Liao, H. B. Schlegel and W. Li, "Disentangling Strong-Field Multielectron Dynamics with Angular Streaking", J. Phys. Chem. Lett. **9**, 2539 (2018).
- ²⁵M. Miranda, C. L. Arnold, T. Fordell, F. Silva, B. Alonso, R. Weigand, A. L'Huillier and H. Crespo, "Characterization of broadband few-cycle laser pulses with the d-scan technique", Opt. Express **20**, 18732 (2012).
- ²⁶D. A. Debrah, G. A. Stewart, G. Basnayake, J. W. G. Tisch, S. K. Lee and W. Li, "Direct in-situ single-shot measurements of the absolute carrier-envelope phases of ultrashort pulses", Opt. Lett. **44**, 3582 (2019).
- ²⁷B. Oguh, E. Orunesajo, S. Abubakar, S. K. Lee and W. Li, "A Time-to-Brightness Converter (TBC): Measuring Photon Arrival Time with Conventional Cameras" (manuscript under review).
- 28 P. H. Bucksbaum, A. Zavriyev, H. G. Muller and D. W. Schumacher, "Softening of the H_2^+ molecular bond in intense laser fields", Phys. Rev. Lett. **64,** 1883 (1990).

PLEASE CITE THIS ARTICLE AS DOI: 10.1063/5.0220000

²⁹M. F. Kling, C. Siedschlag, A. J. Verhoef, J. I. Khan, M. Schultze, T. Uphues, Y. Ni, M. Uiberacker, M. Drescher, F. Krausz and M. J. J. Vrakking, "Control of Electron Localization in Molecular Dissociation", Science **312**, 246 (2006).

³⁰C. Weeraratna, C. Amarasinghe, S. K. Lee, W. Li and A. G. Suits, "Demonstration of multi-hit and multimass capability of 3D imaging in a conventional velocity map imaging experiment", J. Chem. Phys. 149, 084202 (2018).

³¹E. S. Goudreau, A. E. Boguslavskiy, D. J. Moffatt, V. Makhija, M. Hemsworth, R. Lausten, C. Marceau, I. Wilkinson and A. Stolow, "Time-stretched multi-hit 3D velocity map imaging of photoelectrons", Rev. Sci. Instrum. 94, 063002 (2023).

³²A. Nomerotski, M. Brouard, E. Campbell, A. Clark, J. Crooks, J. Fopma, J. J. John, A. J. Johnsen, C. Slater, R. Turchetta, C. Vallance, E. Wilman and W. H. Yuen, "Pixel Imaging Mass Spectrometry with fast and intelligent Pixel detectors", J. Instrum. 5, C07007 (2010).

³³A. T. Clark, J. P. Crooks, I. Sedgwick, R. Turchetta, J. W. L. Lee, J. J. John, E. S. Wilman, L. Hill, E. Halford, C. S. Slater, B. Winter, W. H. Yuen, S. H. Gardiner, M. L. Lipciuc, M. Brouard, A. Nomerotski and C. Vallance, "Multimass Velocity-Map Imaging with the Pixel Imaging Mass Spectrometry (PImMS) Sensor: An Ultra-Fast Event-Triggered Camera for Particle Imaging", J. Phys. Chem. A 116, 10897 (2012).

³⁴A. Zhao, M. v. Beuzekom, B. Bouwens, D. Byelov, I. Chakaberia, C. Cheng, E. Maddox, A. Nomerotski, P. Svihra, J. Visser, V. Vrba and T. Weinacht, "Coincidence velocity map imaging using Tpx3Cam, a time stamping optical camera with 1.5 ns timing resolution", Rev. Sci. Instrum. 88, 113104 (2017).

³⁵L. J. Frasinski, M. Stankiewicz, P. A. Hatherly, G. M. Cross, K. Codling, A. J. Langley and W. Shaikh, "Molecular H₂ in intense laser fields probed by electron-electron, electron-ion, and ion-ion covariance techniques", Phys. Rev. A 46, R6789 (1992).

³⁶L. J. Frasinski, K. Codling and P. A. Hatherly, "Covariance Mapping: A Correlation Method Applied to Multiphoton Multiple Ionization", Science **246**, 1029 (1989).

³⁷A. E. Boguslavskiy, J. Mikosch, A. Gijsbertsen, M. Spanner, S. Patchkovskii, N. Gador, M. J. J. Vrakking and A. Stolow, "The Multielectron Ionization Dynamics Underlying Attosecond Strong-Field Spectroscopies", Science 335, 1336 (2012).